Annu. Rev. Mater. Sci. 1995. 25: 223–47

LASER-INDUCED PHASE TRANSITIONS IN SEMICONDUCTORS

Y. Siegal, E. N. Glezer, L. Huang, and E. Mazur

Division of Applied Sciences and Department of Physics,
Harvard University, Cambridge, Massachusetts 02138

KEY WORDS: femtosecond laser, bandgap collapse, lattice disordering

ABSTRACT

Optical studies of semiconductors under intense femtosecond laser pulse excitation suggest that an ultrafast phase transition takes place before the electronic system has time to thermally equilibrate with the lattice. The excitation of a critical density of valence band electrons destabilizes the covalent bonding in the crystal, resulting in a structural phase transition. The deformation of the lattice leads to a decrease in the average bonding-antibonding splitting and a collapse of the bandgap. We review the relationship between structural, electronic, and optical properties, as well as the timescales for electron recombination, diffusion, and energy relaxation. Direct optical measurements of the dielectric constant and second-order nonlinear susceptibility are used to determine the time evolution of the phase transition.

INTRODUCTION

For almost two decades the field of laser-induced phase transitions in semiconductors has generated considerable interest. This field arose originally in the context of semiconductor annealing, a technologically important process aimed at repairing the damage to semiconductor crystals caused by dopant atom implantation. The conventional method for this process is thermal annealing—the slow baking of a semiconductor in an oven. When the sample is heated, the increased atomic mobility allows

0084–6600/95/0801–0223$05.00

defects to diffuse to the surface. In the 1970s, a new method for repairing damage to semiconductor crystals, now known as laser annealing, was discovered (1). In laser annealing, a short laser pulse incident on a damaged region of a semiconductor induces structural changes in the material that result in the formation of a defect-free crystal. Although laser annealing of semiconductors has not replaced thermal annealing in industrial semiconductor processing, the discovery of laser annealing did open up a new and exciting chapter in the study of light-matter interactions: the use of light to induce phase transitions in semiconductors. Our focus is not on the thermal transition from solid to liquid (melting) induced by nanosecond and picosecond laser pulses, which has been studied in detail. The details of this transition, including the heating of the solid, thermal diffusion, melting, motion of the interphase boundary, and recrystallization are discussed in Reference 2. Instead, we concentrate in this paper on the highly nonequilibrium electronic and structural dynamics in a semiconductor excited by intense femtosecond pulses.

CHEMICAL BONDS AND ENERGY BANDS

The arrangement of atoms in a crystal is intricately connected with the state of the electrons in the material. On one hand, given a set of atoms and their crystal structure, the electronic properties of the solid can be predicted. On the other hand, the valence electrons of the atoms in the solid determine the most energetically favorable arrangement of the ionic cores of the atoms. The cohesion of a semiconductor crystal is primarily due to covalent bonds between the atoms. Because of the periodicity in the crystal structure, there is a corresponding periodicity in reciprocal or crystal momentum space, which allows a useful alternative description of the state of the electrons. In the momentum representation, the spatial description of a bond is replaced by a delocalized representation of the entire electronic system, where the eigenvalues of the Hamiltonian form energy bands. The bond picture of the spatial distribution of electrons and the energy band picture of electronic states in momentum space are two complementary ways of looking at a solid. Although one description may be more appropriate than the other for a particular discussion, an understanding of both pictures provides additional insight into crystal cohesion, electronic properties, and interactions with light.

Figure 1*a* illustrates schematically a covalent bond between two identical atoms, each having only one electron in a particular energy level (note that each level has two spin states). If the two atoms are brought close enough to each other that their wavefunctions overlap, the energies of their collective state will be different from the energies of the individual

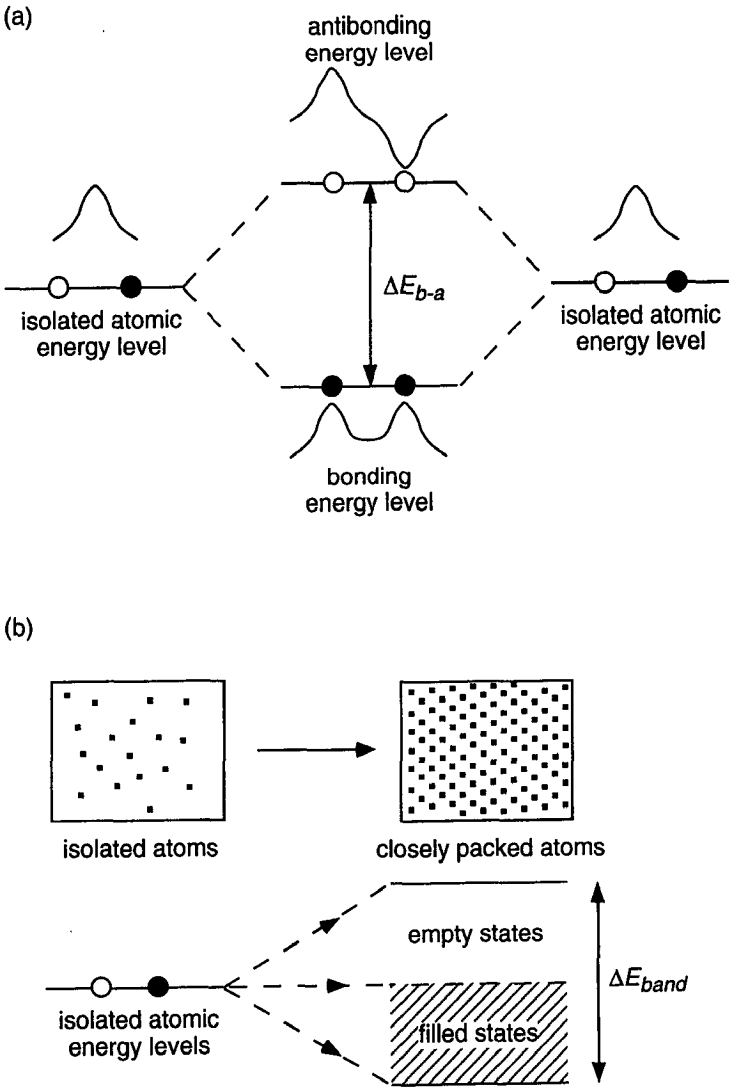

Figure 1 (*a*) Covalent bonding results from the splitting of an atomic energy level into bonding and antibonding levels separated by an energy $\Delta E_{b\text{-}a}$. (*b*) Metallic bonding results from the broadening of an atomic energy level into a band of energies of width ΔE_{band}. ●: filled electronic state, ○: empty electronic state.

atoms. The resulting diatomic molecule has a symmetric ground state wavefunction with an energy lower than the initial atomic level, and an antisymmetric excited state wavefunction with an energy higher than the

initial atomic level. These are called the bonding and antibonding states. The bound configuration consists of two electrons occupying the lower level, where the energy of the molecule is lower than that of the two individual atoms. The sharing of the electrons results in a covalent bond between the two atoms. If one or both of the electrons are excited to the antibonding level, the molecule no longer has a lower total energy than the two individual atoms.

Metallic bonding arises from a more delocalized overlap of atomic orbitals in a solid. This overlap of the orbitals of a particular atomic energy level leads to a broadening of this energy level into a band of energies. If the atomic energy levels are not fully occupied, then, as the atoms are brought closer together to form a solid, the total energy will be lower than for the isolated atoms, as illustrated schematically in Figure 1*b*. This type of bonding results in a partially filled energy band, which is required for electronic conduction and is characteristic of metals (3).

Semiconductors exhibit characteristics of both covalent bonding and metallic bonding. On the one hand, nearest neighbors form covalent bonds by sharing two electrons, which results in a splitting of atomic levels into bonding and antibonding states. On the other hand, these bonding and antibonding states are broadened into bonding and antibonding energy bands by more delocalized interactions with the other atoms in the solid. When the average bonding-antibonding splitting in the material is larger than the width of the energy bands, an energy gap will exist between the bonding and the antibonding bands (see Figure 2*a*). If the atomic orbitals start out half-filled, then the ground state consists of a fully occupied bonding band and an empty antibonding band. In this case, the material will not conduct electricity. However, when the average bonding-antibonding splitting is smaller than the width of the energy bands, the bonding and antibonding bands overlap (see Figure 2*b*). The resulting partially filled bands lead to metallic electronic characteristics even in the ground state. A semiconductor corresponds to the former case: An energy bandgap separates the bonding (valence) and antibonding (conduction) bands. Semiconductors are insulators in the ground state; however, they start conducting when electrons are excited from the valence to the conduction band. Conductivity in a semiconductor is mediated both by the negatively charged electrons excited to the conduction band and by the positive holes left behind in the valence band by the excited electrons. The conducting electrons and holes are often referred to collectively as free charge carriers or simply free carriers.

Most of the work on laser-induced phase transitions has focused on group IV and III–V semiconductors in the diamond and zincblende crystal structures. These materials are appropriate for studying cohesion because

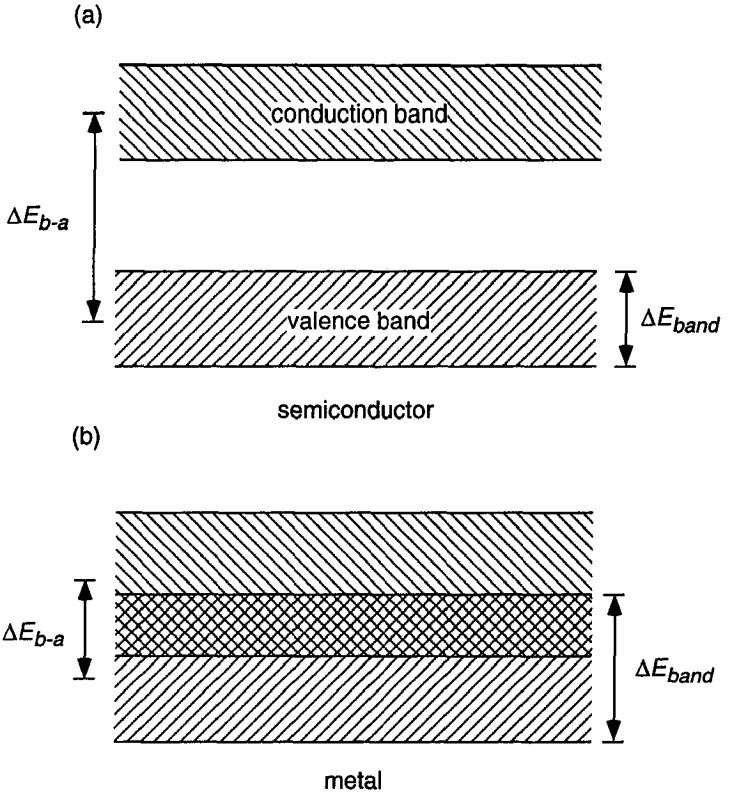

Figure 2 (*a*) Schematic representation of a semiconductor: $\Delta E_{b-a} > \Delta E_{\text{band}}$. (*b*) Schematic representation of a metal: $\Delta E_{b-a} < \Delta E_{\text{band}}$.

of the central role played by covalent bonds in these crystals. Both the diamond and the zincblende structures are built from tetrahedrally coordinated atoms, with each pair of nearest neighbors held together by sharing two electrons. If a significant fraction of these bonding electrons is excited to antibonding states, the cohesion of the crystal will be strongly affected (4).

LIGHT-SEMICONDUCTOR INTERACTIONS

The electronic structure of a material determines its optical properties. Classically, the higher charge-to-mass ratio of the electrons compared with that of the protons in the nucleus accounts for the more important role of the former in the optical response of a material. Quantum mechanically, this dominant role for the electrons arises because optical photon energies

and the energy spacings between electronic levels fall in the same range. The energy spacings between nuclear levels are much larger than optical photon energies, resulting in negligible nuclear transition probabilities. Furthermore, the transition energies for the core electrons are also much greater than optical photon energies, and thus only the valence or outer shell electrons significantly contribute to the optical properties. Although electromagnetic radiation can produce collective vibrational excitations of the lattice by exciting phonons, phonon frequencies are generally in the far infrared, well below the frequencies of interest in this discussion. Thus when visible or ultraviolet light is absorbed by a material, most of the energy is initially transferred to the outer shell electrons without directly perturbing the nuclei or the core electrons.

Absorption of Light in a Semiconductor

Absorption of light in a semiconductor can occur either through interband or intraband electronic excitations. However, an electronic transition can only occur between a filled initial state and an empty final state. In the ground state of a semiconductor (i.e. at absolute zero temperature), all bands are either completely filled or completely empty, so intraband transitions cannot occur. Only when a significant number of electrons has been transferred from the valence to the conduction bands does intraband absorption, also known as free-carrier absorption, become an important mechanism for absorption of light. Usually, interband absorption is the principal mechanism for absorption of light in a semiconductor.

An optically induced interband electronic transition must conserve energy and crystal momentum (4). To satisfy the requirement of energy conservation, the difference between the energies of the final and initial electronic states in the transition $E_{\text{final}} - E_{\text{initial}}$ must equal the energy of the absorbed photon $\hbar\omega$. The magnitude of the momentum of the absorbed photon is much smaller than the magnitude of the electron crystal momentum k. In order to satisfy conservation of crystal momentum, an optically induced electronic transition must leave the electron crystal momentum essentially unchanged. Thus a photon of energy $\hbar\omega$ can directly induce an interband electronic transition only between states that satisfy the condition $E_{\text{final}}(\mathbf{k}) - E_{\text{initial}}(\mathbf{k}) = \hbar\omega$. This type of process, known as a direct transition, is a two-body process involving an electron and a photon. Figure 3a illustrates schematically a direct interband transition.

Interband absorption can also occur through indirect electronic transitions, as shown in Figure 3b. In this case, the initial and final values of the electron crystal momentum are not the same. A phonon is required in the process to carry away the excess momentum. A phonon can have a

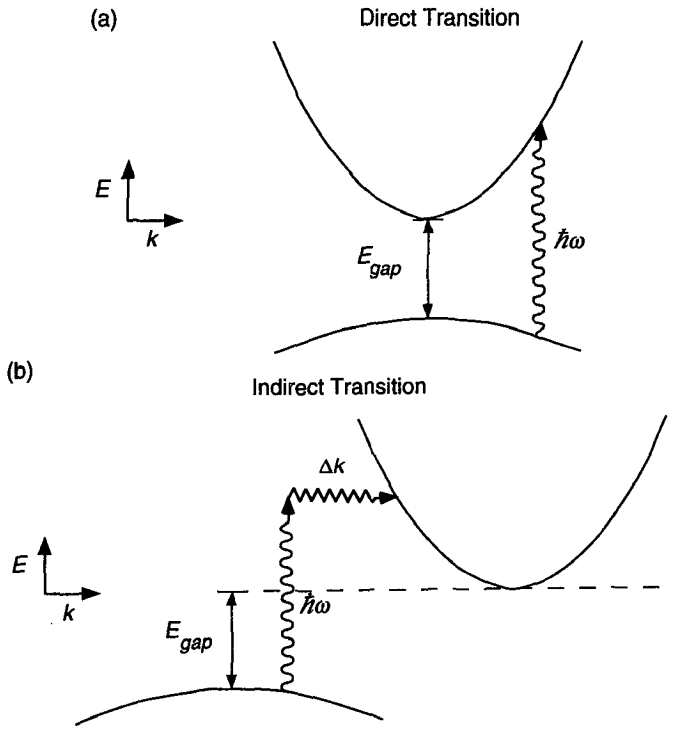

Figure 3 Schematic representation of (*a*) a direct transition and (*b*) an indirect transition. The wiggly arrow represents a photon, and the zig-zag arrow represents a phonon.

large momentum, but its energy is small compared to that of the photon. Thus an indirect transition is characterized approximately by the following two conditions: (*a*) energy conservation, $E_{\text{final}} - E_{\text{initial}} = \hbar\omega_{\text{photon}}$, and (*b*) crystal momentum conservation, $\mathbf{k}_{\text{final}} - \mathbf{k}_{\text{initial}} = \mathbf{k}_{\text{phonon}}$. Because direct transitions are lower-order processes than indirect transitions, direct transitions dominate the absorption spectrum over the range of photon energies in which they are allowed.

There are several common features in the absorption spectra of semiconductors that result from common features in their band structures. One of the most noteworthy features is the fundamental absorption edge at a photon energy corresponding to the minimum energy gap E_{gap} separating the valence and conduction bands. Assuming negligible free-carrier absorption, a semiconductor is transparent to light of photon energy

less than E_{gap} because there are no resonant interband transitions in this frequency range, as shown in Figure 3.[1]

At photon energies above E_{gap}, the absorption spectrum will depend on whether a semiconductor has a direct or an indirect minimum bandgap. In a direct-gap semiconductor such as GaAs, the minimum in the conduction band occurs at the same point in k-space (same value of crystal momentum) as the maximum in the valence band. In contrast, the conduction band minimum and the valence band maximum occur at different points in k-space for an indirect semiconductor such as Si. Thus direct transitions dominate the absorption spectrum of direct-gap semiconductors at all photon energies above E_{gap}. Indirect transitions make up the absorption spectrum of indirect-gap semiconductors at photon energies between E_{gap} and the minimum value of the direct energy gap $E_{conduction}(\mathbf{k}) - E_{valence}(\mathbf{k})$ (see Figure 3b).

In general, the conduction band of a semiconductor has more than one relative energy minimum in k-space. The absolute conduction band minimum in GaAs occurs at $\mathbf{k} = 0$, known as the Γ-point. The region around this minimum is called the Γ-valley. GaAs also has relative minima at points symmetrically equivalent to $\mathbf{k} = (111)\pi/a$ and $\mathbf{k} = (100)\pi/a$, where a is the lattice spacing. The eight symmetrical equivalents of $\mathbf{k} = (111)\pi/a$ are known as L-points, whereas the six symmetrical equivalents of $\mathbf{k} = (100)\pi/a$ are called the X-points. The regions around these symmetry points are called the L-valleys and the X-valleys, respectively. In GaAs at room temperature, the direct energy gap at the Γ-point, which is also the minimum energy gap E_{gap}, is equal to 1.42 eV (6). Pseudopotential calculations show the direct gaps at the L- and X-points to be about 3 and 5 eV, respectively (7). Also, the conduction-band minimum at the L-point is 0.29 eV above that at the Γ-point, whereas the X-point conduction-band minimum exceeds that at the Γ-point by 0.48 eV (6). Figure 4 shows the band structure of GaAs between the L- and Γ-points and between the Γ- and X-points.

The optical properties of a semiconductor are quantitatively described by the dielectric function $\varepsilon(\omega)$. The dielectric function is complex and describes the magnitude and phase of the material response to an electromagnetic field. Figure 5 shows both the real and imaginary parts of the dielectric function of GaAs at room temperature (8). The three main features, labeled E_{gap}, E_1, and E_2, are common to the Group IV and III–V semiconductors, although their locations and the relative sizes of these

[1] Discrete absorption lines, however, do appear a few meV below E_{gap} that correspond to the excitation of bound electron-hole pairs of excitons (5).

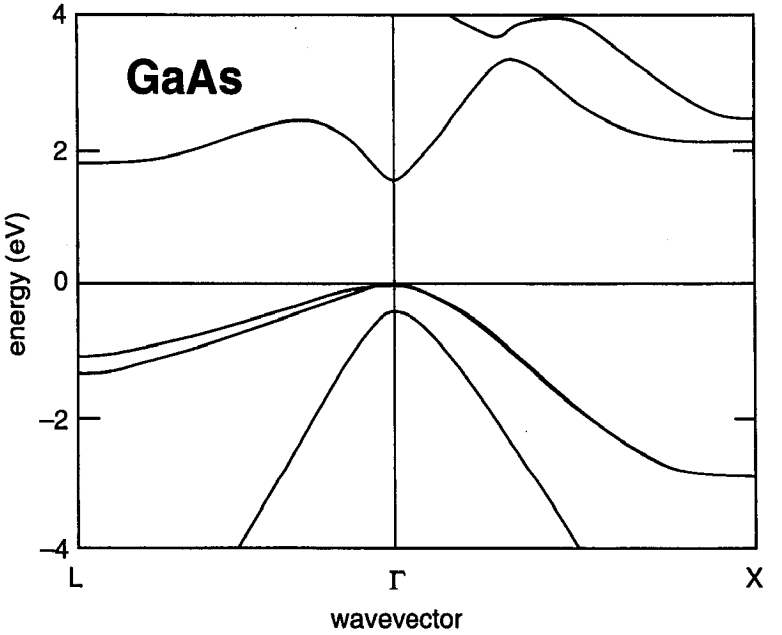

Figure 4 A section of the electronic band structure of GaAs (after Reference 7).

features vary from material to material. The point E_{gap} (at 1.42 eV for GaAs) marks the fundamental band edge below which Im(ε) is zero; E_1 and E_2 (located at 3.0 eV and 4.75 eV, respectively, for GaAs) (9) label the two main absorption peaks in the spectrum. These peaks arise from regions in the band structure (the region around the L-point for the E_1 peak and the region around the X-point for the E_2 peak) in which the valence band is roughly parallel to the conduction band, resulting in a large, joint density of states for direct interband transitions (10). The E_2 peak, which is roughly coincident with the zero-crossing in Re(ε), is the stronger of the two absorption peaks, and its location gives the approximate value of the average bonding-antibonding splitting of GaAs (3).

Much of the work on laser-induced phase transitions discussed in this paper involves the optical excitation of GaAs at photon energies above E_{gap}. Because GaAs is a direct-gap semiconductor, the optical excitation is dominated by direct transitions at all frequencies. Although there are differences in the details of optical excitation in direct-gap vs indirect-gap semiconductors, most of the key issues we address apply to both types of materials. Analysis of the results presented here for GaAs, however, is simplified by the lack of complications arising from indirect transitions.

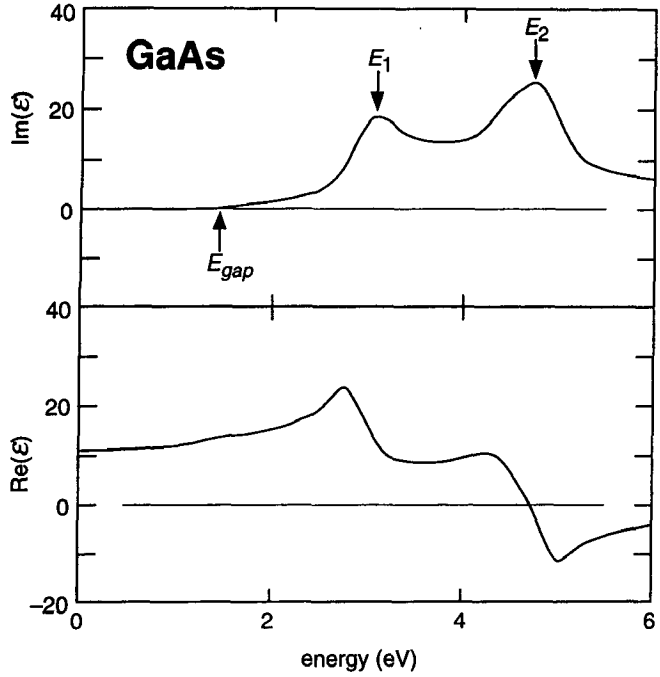

Figure 5 Dielectric function of GaAs (after Reference 8). E_{gap} labels the fundamental absorption edge corresponding to the minimum bandgap. E_1 and E_2 label the two main absorption peaks.

Energy Transfer in a Semiconductor

The optical excitation of electrons from the valence band to the conduction band in a semiconductor leads to a series of processes through which the energy of the excited electrons is distributed to the rest of the electronic system as well as to the lattice. Figure 6 summarizes the main energy transfer processes. Optical excitation of electrons can occur only in regions of k-space satisfying the direct transition condition $E_{\text{final}}(\mathbf{k}) - E_{\text{initial}}(\mathbf{k}) = \hbar\omega$, where ω is within the spectral bandwidth of the incident light. As a result, the incident light creates a nonequilibrium population of free carriers (electrons in the conduction band and holes in the valence band) with a narrow distribution of crystal momentum (localized in k-space).

CARRIER–CARRIER SCATTERING The nonequilibrium free-carrier population quickly spreads out in k-space through carrier–carrier scattering, as indicated by process 1 in Figure 6. The time scale for electron–electron scattering decreases with increasing conduction electron density and is

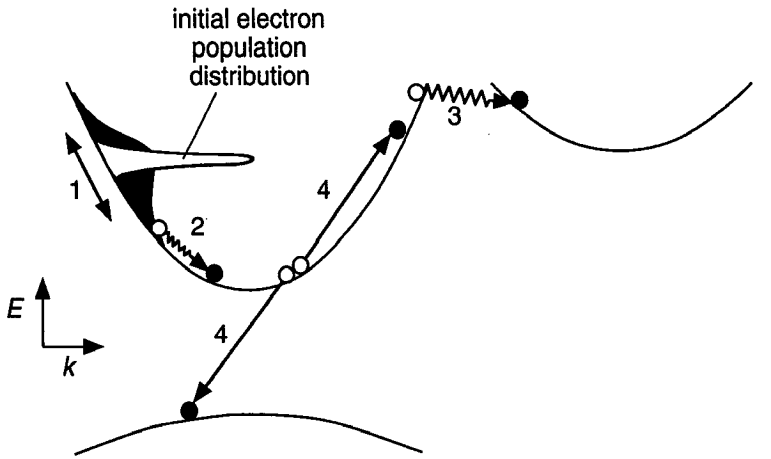

Figure 6 Representation of scattering processes and their corresponding equilibration times following laser excitation of an initial distribution of free carriers. Process 1 indicates the spreading out of the initial carrier distribution in k-space through carrier-carrier scattering, which leads to carrier thermalization. Processes 2 and 3 show intravalley and intervalley carrier-phonon scattering, respectively. The interaction of carriers and phonons leads to electron-lattice equilibration. Carrier-density relaxation occurs through recombination processes such as Auger recombination, shown by process 4. In Auger recombination, an electron and a hole recombine, giving off the excess energy and momentum to a third free carrier.

shorter than 20 fs for electron densities in excess of 10^{18} cm^{-3} (11). Through multiple scattering, the initial nonequilibrium distribution of free carriers thermalizes to a Fermi-Dirac distribution within a few hundred femtoseconds (12). The temperature of this thermal distribution is set by the initial free-carrier excess energy, corresponding to the energy above the conduction band minimum for electrons and the energy below the valence band maximum for holes. Thus carrier–carrier scattering merely redistributes the energy among the excited electrons and holes and does not change the average energy of the excited free carriers.

Carrier–carrier scattering includes three similar but separate processes: electron–electron scattering, hole–hole scattering, and electron–hole scattering. The first two lead to independent thermalization of the excited electron and hole populations, whereas the third leads to equilibration of the two populations with each other. Electron–hole equilibration is driven by the initial difference in average excess energies between excited electrons and holes. In GaAs, for example, a difference between electron and hole excess energies arises during direct interband transitions in the Γ-valley because of the higher curvature of the conduction band compared with that of the valence band (see Figure 3*a*).

CARRIER-PHONON SCATTERING Although the excited free carriers become internally thermalized within a few hundred femtoseconds, they are still far out of equilibrium with the lattice on this time scale. Energy transfer from the excited electrons to the lattice occurs through the slower process of carrier–phonon scattering, shown by process 2 in Figure 6. The time scale for carrier–phonon scattering is longer than that for carrier–carrier scattering because the coupling of free carriers to phonons is weaker than the coupling of free carriers to each other. Typical carrier–phonon scattering times are on the order of a few hundred femtoseconds (13). However, multiple scattering is required to transfer the excess energy from the electrons to the lattice. The phonons primarily responsible for cooling the hot electrons have energies on the order of 30 meV (see below). For initial electron excess energies on the order of 0.5 eV (corresponding to excitation of GaAs with 2-eV photons), the energy transfer process requires over 10 phonon emission events per electron. Thus for excitation significantly above the bandgap, electron-lattice thermalization occurs on a time scale of a few picoseconds (13).

Before describing the interactions between free carriers and phonons, we first examine the phonon spectrum of semiconductors, shown schematically in Figure 7. Because diamond (Si) and zincblende (GaAs) crystal lattices have a two-atom basis, the phonon spectra of these materials split into two main branches: acoustic and optical (4). Each of these branches in turn splits into three polarization vectors for the atomic displacements of a traveling wave: two that are transverse to the direction of propagation and one that is longitudinal. The acoustic branch gets its name from the small wavevector limit in which it has a linear dispersion relation and supports the propagation of sound. The optical branch has higher frequencies than the acoustic branch and a relatively flat dispersion relation. It is called the optical branch because its small wavevector phonons can couple directly to infrared photons. Although free carriers can interact with both optical and acoustic phonons, energy transfer is dominated by optical phonons because of their higher energies.

The nature of the interaction between free carriers and phonons in semiconductors depends on whether there is an ionic component to the crystal bonding. In an elemental semiconductor such as Si, the bonds are purely covalent, and the carrier-phonon interaction is mediated by the deformation potential (5), which is the potential energy associated with the change in electronic band structure arising from small atomic displacements produced by lattice vibrations. This change in band structure introduces an effective force between phonons and free carriers. The deformation potential coupling is independent of phonon wavevector (5), allowing hot free carriers to emit phonons of different wavelengths.

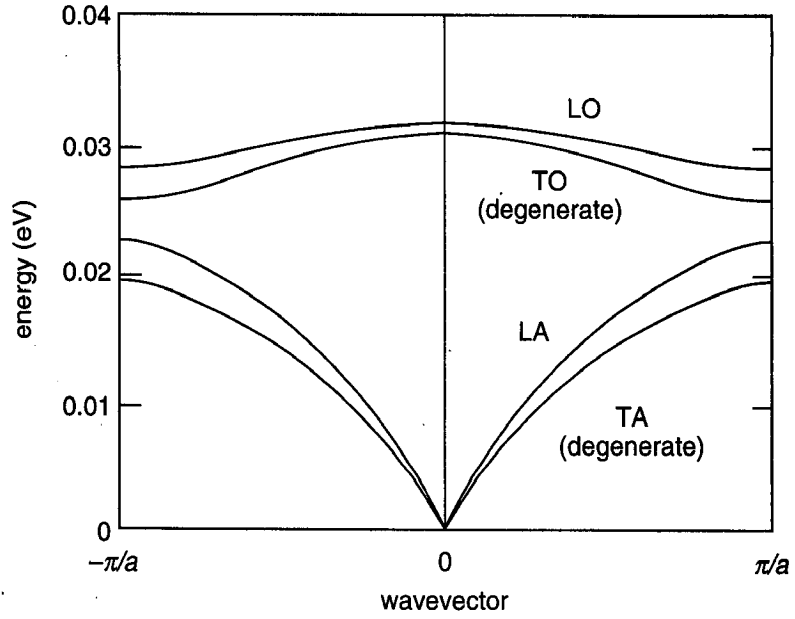

Figure 7 Typical phonon spectrum along a symmetry direction for a crystal with a two-atom basis and cubic symmetry. LO: longitudinal optical modes; TO: transverse optical modes; LA: longitudinal acoustic modes; TA: transverse acoustic modes.

Compound semiconductors such as GaAs, on the other hand, have partially ionic bonds because of the different electron affinities of the two component elements. In this type of material, known as a polar semiconductor, the atomic displacements of a phonon set up an oscillating electric dipole. For longitudinal lattice vibrations, this dipole gives rise to an electric field that couples directly to the charged free carriers (14). The polar coupling is inversely proportional to the square of the phonon wavevector (5), leading to preferential emission of long-wavelength phonons by hot free carriers. Because the longitudinal optical (LO) phonons emitted by electrons through the polar interaction have long wavelengths (small values on q, the phonon wavevector), the change in electron crystal momentum is very small. This small change in crystal momentum means that after emitting an LO phonon, the conduction-band electron remains within the same energy valley as that of its initial state. In GaAs, electronic cooling occurs mainly through intravalley phonon scattering.

Intervalley phonon scattering can also play an important role in energy transfer following the optical generation of free carriers (15). In intervalley scattering, illustrated by process 3 in Figure 6, excited electrons scatter

into a different conduction band valley through either phonon emission or absorption. Because the various conduction band valleys are centered at different values of crystal momentum, intervalley scattering requires large q (short wavelength) optical or acoustic phonons to satisfy the requirement of crystal momentum conservation. Thus the deformation potential mediates this type of scattering. Note that intervalley scattering will not occur for an electron if its energy is more than a phonon quantum below the minimum of the destination valley.

By distributing the excited electron population throughout the conduction band, intervalley scattering affects the electron-lattice energy relaxation time. In the experiments on GaAs reviewed in this paper, a laser pulse excites electrons primarily into the Γ-valley. However, intervalley scattering transfers some of these excited electrons into the L- and X-valleys, both of which have higher energy minima than the Γ-valley. Because they do not have as far to decay, the electrons in these side valleys cannot emit as many LO phonons through polar scattering as the electrons in the Γ-valley unless they scatter back into the Γ-valley. In this way, intervalley scattering slows down the transfer of energy from the electronic system to the lattice (15).

CARRIER RECOMBINATION AND DIFFUSION Although the scattering processes discussed so far distribute the initial excitation energy throughout the electronic system and the lattice, none of these processes changes the density of the excited free carriers. Two processes that do change the free-carrier density are carrier recombination and carrier diffusion. Carrier recombination, or electron-hole recombination, refers to processes in which an electron in the conduction band and a hole in the valence band recombine. In other words, an electron previously excited to the conduction band makes a transition back down to the valence band, as shown by process 4 in Figure 6. Carrier diffusion, on the other hand, refers to the average motion of free carriers from high carrier-density regions to low carrier-density regions. Recombination lowers the total number of free carriers in a crystal whereas diffusion redistributes free carriers in real space. However, for the purposes of the work reviewed in this paper, both types of processes reduce the number of free carriers in the laser-excited region.

Time scales for recombination processes depend on the free-carrier density and on the specific type of process. The various types of recombination differ according to how the energy lost by the electron in the downward transition to the valence band is given off. Two of the most important types of recombination are radiative recombination, in which the transition energy is radiated as a photon, and Auger recombination, in which the transition energy is transferred to another free carrier.

A radiative recombination event occurs through the spontaneous emission of a photon when a conduction band electron and a valence band hole annihilate each other. Thus the radiative recombination rate $R_{\text{radiative}}$ is proportional to the product of the conduction electron density times the hole density: $R_{\text{radiative}} = C_{\text{radiative}}np$, where n is the conduction electron density, p is the density of holes in the valence band, and $C_{\text{radiative}}$ is a constant (16). In the case of optical generation of free carriers, $n = p = N$, where N is the density of electron-hole pairs. We can define an instantaneous recombination time $\tau_{\text{radiative}}$ by setting $R_{\text{radiative}} = N/\tau_{\text{radiative}}$. Then for radiative recombination, we have $\tau_{\text{radiative}} = (C_{\text{radiative}}N)^{-1}$.

In contrast, an Auger recombination even involves three free carriers because the electron-hole annihilation transfers energy either to another conduction electron or to a hole in the valence band. Therefore, the Auger recombination rate R_{Auger} in the case of optically generated free carriers with density N is given by $R_{\text{Auger}} = C_{\text{Auger}}N^3$. This expression gives an instantaneous Auger recombination time of $\tau_{\text{Auger}} = C_{\text{Auger}}^{-1}N^{-2}$. In laser-induced structural change experiments using femtosecond-excitation pulses, the femtosecond laser pulse generates initial carrier densities greater than 10^{21} cm^{-3}, a regime where Auger recombination is the dominant mechanism (17).

The above treatment of recombination needs to be modified at high carrier densities where $C_{\text{radiative}}$ and C_{Auger} themselves become functions of N. Once N exceeds roughly 10^{18} cm^{-3}, both of these coefficients will decrease with increasing carrier density due to electronic screening effects. The presence of many mobile charge carriers leads to a partial screening of the Coulomb interaction between free carriers. The weaker interaction reduces the probability of a recombination event, thus lowering the recombination rate compared to the unscreened case. A calculation based on static screening theory for the case of Si suggests that the Auger recombination time saturates at about 6 ps for carrier densities exceeding 10^{21} cm^{-3} (17).

Carrier diffusion is another important mechanism that reduces the free carrier density in the region excited by the laser pulse. The rate at which carriers diffuse out of the laser-excited region is given by $R_{\text{diffusion}} = N/\tau_{\text{diffusion}} = D_a\nabla^2 N$, where the ambipolar diffusion constant D_a takes into account diffusion of both electrons and holes (5). If the laser spot size on the sample surface is much bigger than the absorption depth δ, then the carrier density varies only in the direction normal to the sample surface: $N(z) = N(0)e^{-z/\delta}$. In this case, the diffusion time is given by $\tau_{\text{diffusion}} = \delta^2/D_a$. The diffusion constant D_a is related to the excited electron temperature T_e and to the carrier mobility through the Einstein relation $D_a = k_B T_e \mu_a/e$ (5, 17), where k_B is the Boltzmann constant, μ_a a reduced carrier mobility for

conduction electrons and valence holes, and e is the magnitude of the electron charge. If the electron temperature varies in time, such as during and after femtosecond laser-pulse excitation (18), the diffusion constant will also vary in time. The dependence of D_a on electronic temperature is further complicated by the implicit dependence of the carrier mobility μ_a on the electron temperature, which is not easily determined.

Although an increased electron temperature resulting from femtosecond laser-pulse excitation should speed up diffusion, carrier confinement slows it down (18). This effect arises from the reduction in the bandgap in an excited semiconductor due to many-body interactions in the free-carrier system (18, 19). In laser-pulse excitation, the spatial gradient of the light intensity in the material leads to a spatial gradient in the excited carrier density. The carrier-density gradient, in turn, causes a gradient in the bandgap, with a smaller bandgap coinciding with higher carrier density. In the absence of diffusion, free carriers will tend towards the regions with smaller bandgaps, thus this spatial gradient results in carrier confinement that slows down diffusion (18). Simulations and experimental measurements show that carrier-density relaxation through these processes occurs on a picosecond time scale (17, 18, 20, 21).

SUMMARY OF ENERGY TRANSFER The above discussion of energy transfer in a semiconductor is not meant to be a comprehensive treatment of this expansive subject. Many other scattering mechanisms such as scattering with plasmons (collective electronic excitations), impurity scattering, and combinations of all of the above play a role in the distribution of the laser-deposited energy. A full review of these processes can be found in Reference 4. The goal of this section is to provide a sense for the relevant time scales for energy transfer following femtosecond laser-pulse excitation of a semiconductor. In particular, carrier–carrier scattering thermalizes the free–carrier population within a few hundred femtoseconds; carrier-phonon scattering leads to carrier–lattice equilibration on a time scale of a few picoseconds; and carrier recombination and diffusion reduce the free-carrier density in the excited region also within a few picoseconds.

LASER-INDUCED PHASE TRANSITIONS

The strong connection between the electronic system and the lattice structure of a solid suggests that a change in one affects the other. When a laser pulse is incident on a semiconductor, it interacts with the electronic system in the material by exciting electrons from the valence band to the conduction band. If strong enough, this electronic excitation leads to a struc-

tural change in the lattice. The central question to address, then, is how the excitation of the electronic system results in atomic motion.

Thermal Model vs Plasma Model

Following the first experiments in laser annealing, two models were proposed to explain the structural change resulting from electronic excitation. One model, known as the thermal model, describes the structural change as a thermal melting process (22–24). The thermal model assumes that the hot electrons rapidly equilibrate with the lattice by exciting lattice vibrations (emitting phonons). With this assumption, the laser energy deposited in the material can be treated as though it is instantly converted to heat. If the incident laser pulse is strong enough, the irradiated part of the sample will heat up to the melting temperature and undergo a transition to the liquid phase as the latent heat of fusion is supplied.

The other model, known as the plasma model, attributes the structural change to destabilization of the covalent bonds resulting directly from the electronic excitation (25, 26). The plasma model assumes a slow rate of phonon emission by the excited electronic system compared with the energy deposition time (i.e. the laser pulse width). This assumption implies that structural change can occur while the electronic system and the lattice are not in thermal equilibrium with each other, although each of these systems may be internally in a quasi-equilibrium. According to this model, the structural change is driven directly by the excited electronic system. If a high enough fraction of the valence electrons is excited from bonding states to antibonding states, the crystal becomes unstable, and a structural phase transition occurs.

Picosecond Pulses vs Femtosecond Pulses

The debate over the explanation for laser-induced structural change prompted experimental tests of these two models. Early results, from experiments involving laser pulses with pulse widths of tens of picoseconds or longer, showed evidence for strong heating of the sample and agreed well with predictions from computer simulations based on the thermal model (22, 27, 28). Later, Raman spectroscopy experiments on semiconductors confirmed that an excited electronic system can equilibrate with the lattice in just a few picoseconds (13), in agreement with the assumption in the thermal model.

The introduction of femtosecond lasers in the mid-1980s led to renewed interest in this topic (29). The development of lasers producing pulses of less than 100 fs duration opened up the possibility of depositing energy in a semiconductor on a time scale that is short compared with the electron-

lattice equilibrium time of a few picoseconds. By depositing energy faster than the electrons can transfer it to the lattice or recombine with holes, an intense short pulse can excite a very high density of free carriers before significant heating of the lattice can occur. Due to the high peak intensities in femtosecond pulses, nonlinear absorption further increases the density of excited carriers (30). This suggests that femtosecond laser-pulse excitation of semiconductors can create the conditions necessary for electronically driven structural change. Indeed, recent experimental results show that the response of a semiconductor to a femtosecond laser pulse is fundamentally different from the response to a picosecond or nanosecond laser pulse (29, 31–38). The remainder of this paper focuses on the femtosecond excitation-pulse regime.

Response of the Linear Optical Properties

Determining the behavior of both the electronic and structural properties of a semiconductor is of prime importance to understanding the phase transition induced by a femtosecond optical excitation. However, to probe the structural change directly would require a subpicosecond X-ray or electron probe, which is not currently available. To resolve the response of a material to laser-pulse excitation on such a short time scale, a femtosecond laser pulse is generally used to probe the optical properties of the material over a range of time delays following the excitation pulse. In essence, this pump-probe technique provides a series of snapshots of the material at different times following the excitation, thereby mapping out the time evolution of the optical property being measured. Because the optical properties of a semiconductor are directly related to its electronic structure, as discussed above, optical pump-probe techniques provide a valuable tool for monitoring the changes in the electronic band structure. The band structure in turn carries information about the crystal structure.

Using this pump-probe scheme, a number of researchers have mapped out the time evolution of a semiconductor's reflectivity following intense femtosecond laser-pulse excitation (29, 31–33, 35–38). In both Si (29, 31–33) and GaAs (35–37), the reflectivity shows a sharp rise within roughly 200 fs after the excitation pulse for excitation fluences greater than the threshold for permanent damage. Figure 8 shows a typical example of this reflectivity behavior plotted vs pump-probe time delay. The data points in Figure 8 represent experimental values for the reflectivity of GaAs at a 45° incident angle for *p*-polarized light measured using a 70-fs, 2.2-eV probe pulse following excitation with a 70-fs 1.9-eV excitation pulse. The fluence (energy per unit area) of the excitation pulse in this case is 1.5 kJ/m^2. This is 1.5 times greater than the measured damage threshold of 1.0 kJ/m^2 for GaAs (39). In the past, the increase in reflectivity seen in Figure 8 was

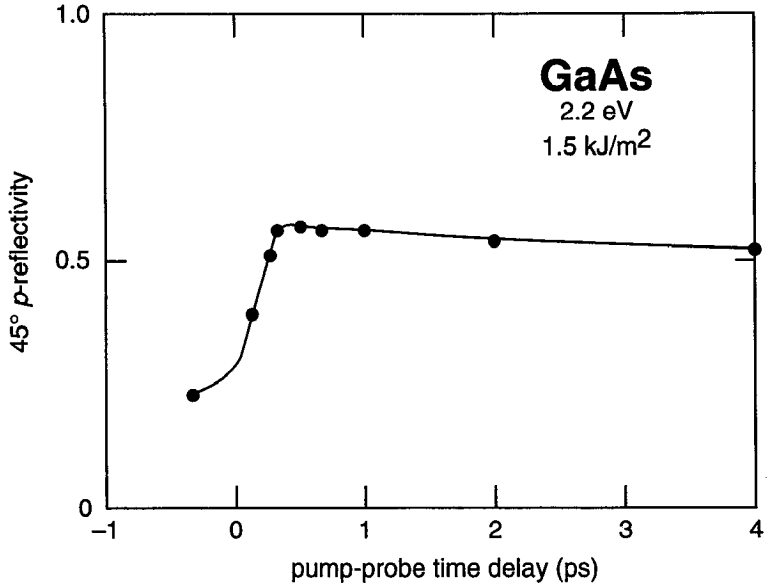

Figure 8 Measured reflectivity of GaAs at 45° incident angle for *p*-polarized, 2.2-eV light following excitation with a 70-fs, 1.5-kJ/m^2, 1.9-eV laser pulse. The reflectivity values are plotted vs the time delay between the arrival of the excitation pulse and the arrival of the probe pulse. The curve through the data is drawn to guide the eye.

attributed to the metallic-like behavior of the excited free carriers. Because the time scale for the reflectivity rise is about an order of magnitude shorter than the time scale for heating of the lattice through phonon emission (see above section), this change cannot be driven by thermal processes.

The reflectivity data alone, however, do not provide a clear link to the changes in the electronic structure induced by the excitation pulse because reflectivity measurements made at a single angle of incidence and polarization do not unambiguously determine the induced changes in the semiconductor's linear optical properties. The ambiguity in interpreting reflectivity data arises because reflectivity is not an intrinsic material property. Rather, it is a function of both the real and imaginary parts of the linear optical susceptibility or, equivalently, the dielectric constant. It is the response of the dielectric constant that provides a clear link to the behavior of the electronic structure. One can unambiguously determine both the real and imaginary parts of the dielectric constant by using two synchronized probe pulses to simultaneously measure the reflectivity at two carefully chosen angles of incidence and polarizations (40).

Recent pump-probe measurements of the dielectric constant made using this type of two-angle reflectivity technique show that the reflectivity

behavior described above reflects a drop in the average bonding-antibonding splitting of the semiconductor, leading to a collapse of the bandgap (39, 41, 42). The average bonding-antibonding splitting of a material manifests itself optically as the resonant frequency of the main absorption peak in its spectrum (10). Thus the drop in the average splitting is accompanied by a drop in the resonant frequency of the main absorption peak. As this resonant frequency drops through the frequency of the probe pulse, the imaginary part of the dielectric constant at the probe frequency goes through a peak, while the real part crosses zero. Figure 9, which shows experimental values for the real and imaginary parts of the dielectric constant of GaAs at a photon energy of 2.2 eV plotted vs pump-probe time delay, illustrates this behavior. As in Figure 8, the excitation pulse is a 70-fs 1.9-eV laser pulse with a fluence of 1.5 kJ/m^2. Note that the imaginary part peaks and the real part crosses zero within a few hundred femtoseconds, indicating that within this time, the average bonding-antibonding splitting has dropped from its initial value of about 4.5 eV to below 2.2 eV. This evolution of the dielectric constant produces the rise in

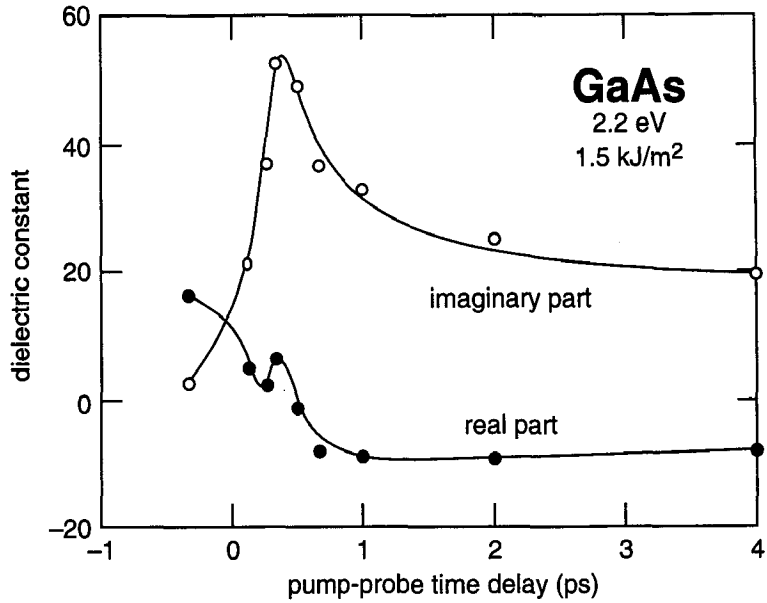

Figure 9 Experimentally determined 2.2-eV dielectric constant of GaAs plotted vs pump-probe time delay. As in Figure 8, a 70-fs, 1.5-kJ/m^2, 1.9-eV laser pulse serves as the pump pulse. The curves through the data are drawn to guide the eye. ●: real part of the dielectric constant, ○: imaginary part of the dielectric constant.

the reflectivity seen in Figure 8. Less intense pulses, down to a fluence of 0.8 kJ/m^2, produce a similar drop in the resonant frequency of the main absorption peak, but on a slower time scale.

The large changes in the electronic band structure evident in the dielectric constant measurements most likely arise from a combination of electronic screening by the excited free carriers and structural deformation of the lattice resulting from an electronically induced lattice instability. The free carriers generated by the laser pulse modify the electronic band structure directly through many-body interactions and by screening the ionic potential. A recent calculation shows that these screening effects cause a 2-eV drop in the direct gap at the X-point in GaAs if 10% of the valence electrons are excited to the conduction band—roughly the free-carrier density attained by femtosecond excitation pulses in these experiments (43). However, the time scale for the drop in the average bonding-antibonding splitting indicates that electronic screening cannot account for the entire bandgap collapse. Screening should be largest immediately following the excitation, i.e. when the free-carrier density is highest. As the free-carrier density relaxes through Auger recombination and diffusion, the changes in the electronic band structure due to screening should also relax. Instead, when excited by pulses of about 1.0 kJ/m^2 fluence, the average bonding-antibonding splitting continues to drop for picoseconds following the excitation. Thus while electronic screening is an important effect immediately following the excitation, the changes in the electronic band structure occurring during the first few picoseconds must be due to changes in the lattice structure itself.

As discussed in the first section of this paper, the covalent bonds that hold a semiconductor together are only stable if the electrons are in the ground state. Excitation of electrons from bonding valence states to antibonding conduction states breaks the covalent bonds. If enough bonds are broken, the lattice structure will become unstable, i.e. certain phonon modes will become soft, and the lattice will begin to deform. Thus a femtosecond laser pulse can induce a lattice instability if it excites a critical density of electrons, which calculations put at roughly 10% of the valence electrons (25, 44, 45). Under these conditions, these ions can move a significant fraction of the bond length within a few hundred femtoseconds (45, 46). Since a 10% change in the average bond length is sufficient for the bandgap to collapse (47), this ionic motion can result in a semiconductor-metal transition on a time scale consistent with the experimental data described above. This interpretation of the behavior of the linear optical properties is further supported by experimental data on the behavior of the nonlinear optical properties, which are discussed below.

Response of the Second-Order Optical Susceptibility

The symmetries of a material play an important role in determining its nonlinear optical properties (48). Thus monitoring the behavior of these properties can provide useful information on changes in the lattice structure. In particular, because of its sensitivity to crystal structure, second-harmonic generation has been used as a probe during laser-induced phase transitions in both the picosecond (49–51) and in the femtosecond regimes (33–37, 52). The central idea in most of this work is that the second-order optical susceptibility, which is responsible for second-harmonic generation in the dipole approximation, is only non-zero in materials that lack inversion symmetry (48). In fact, ion implantation experiments show that a loss of long-range order, which in effect produces inversion symmetry on the scale of the wavelength of light, is enough to make the second-order optical susceptibility vanish (53). Thus in pump-probe experiments on GaAs, which lacks inversion symmetry, a drop to zero in the second-harmonic signal indicates a loss of long-range order (52, 54).[2] It is important to note that extracting the true behavior of the second-order susceptibility from measurements of the generated second-harmonic signal requires a knowledge of the changes in the linear properties (52, 54). For femtosecond laser-pulse excitation of semiconductors at fluences above the damage threshold, second-harmonic generation has been observed to vanish on a time scale of about 100 fs following the excitation (33, 36, 55). This behavior supports the conclusion that a deformation of the lattice causes the collapse of the bandgap within a few hundred femtoseconds. In GaAs, the second-order optical susceptibility has been observed to drop to zero even at fluences below the damage threshold, which indicates that there is a range of fluences at which the laser excitation results in a reversible loss of long-range order (54).

Combining the experimental data on the second-order optical susceptibility with that on the linear optical properties provides a self-consistent picture of the effects of the femtosecond laser-pulse excitation on the semiconductor. The excitation of a critical density of electrons from the valence band to the conduction band destabilizes the covalent bonds in the material. The ionic motion resulting from this laser-induced lattice instability leads to a loss of long-range order in the lattice structure, evident in the drop to zero of the second-harmonic signal. The deformation of the

[2] Although Si has inversion symmetry, second-harmonic generation can still be a useful tool for monitoring long-range order with a proper orientation of the crystallographic axes and probe beam polarization. In this case, second-harmonic generation arises from an order-dependent quadrupole term in the second-order nonlinear polarization (33).

lattice is accompanied by the drop in the average bonding-antibonding splitting seen in the resonance behavior of the dielectric constant.

CONCLUSION

Determining the behavior of the optical properties of semiconductors during laser-induced phase transitions provides a window on the complex interplay between the electronic structure and lattice structure of the material. By exciting a high density of electrons from the valence band to the conduction band, an intense femtosecond laser pulse can destabilize the covalent bonds of the semiconductor. The creation of the required density of free carriers is made possible by the very short time during which the energy is deposited into the electronic system. The deformation of the lattice structure that is driven by the electronic excitation in turn changes the electronic band structure, leading to a drop in the average bonding-antibonding splitting and a transition to metallic behavior.

While much has been learned about laser-induced phase transitions in semiconductors since the discovery of laser annealing, many questions remain to be answered. For example, what are the details of the bandgap collapse? Can we distinguish more clearly the role of electronic screening from that of lattice deformation in modifying the electronic band structure? What does the deformed lattice look like? What are the lattice relaxation dynamics at fluences below the damage threshold? Remaining issues such as these promise to keep this a stimulating field of research.

ACKNOWLEDGMENTS

We appreciate many useful discussions with Professors N. Bloembergen, H. Ehrenreich, E. Kaxiras, and M. Aziz. E.N.G. gratefully acknowledges a Fannie and John Hertz Fellowship. We would also like to acknowledge financial support from the Joint Services Electronics Program under contract number ONR N00014–89-J-1023 and the National Science Foundation under contract number NSF DMR 89–20490.

Literature Cited

1. Shtyrkov EI, Khaibullin IB, Zaripov MM, Galyatudinov MF, Bayazitov RM. 1976. *Sov. Phys. Semicond.* 9: 1309
2. Biegelsen DK, Rozgonyi GA, Shank CV, eds. 1985. *Energy Beam-Solid Interactions and Transient Thermal Processing*. Vol. 35. Pittsburgh: Mater. Res. Soc.
3. Harrison WA. 1989. *Electronic Structure and the Properties of Solids: The Physics of the Chemical Bond*. New York: Dover
4. Ashcroft NW, Mermin ND. 1976. *Solid State Physics*. Philadelphia: Saunders
5. Seeger K. 1991. *Semiconductor Physics: An Introduction*. Berlin: Springer-Verlag
6. Pierret RF. 1987. *Advanced Semiconductor Fundamentals*. Reading, MA: Addison Wesley
7. Chelikowsky JR, Cohen ML. 1976. *Phys. Rev. B* 14: 556
8. Palik ED. 1985. In *Handbook of Optical Constants of Solids*, ed. ED Palik, pp. 429–43. New York: Academic
9. Aspnes DE, Schwartz GP, Gualtieri GJ, Studna AA, Schwartz B. 1981. *J. Electrochem. Soc.* 128: 590
10. Cohen ML, Chelikowsky JR. 1988. *Electronic Structure and Optical Properties of Semiconductors*. Berlin: Springer-Verlag
11. Conwell EM, Vassel MO. 1966. *IEEE Trans. Electron. Devices* 13: 22
12. Goldman JR, Prybyla JA. 1994. *Phys. Rev. Lett.* 72: 1364
13. Kash JA, Tsang JC, Hvam JM. 1985. *Phys. Rev. Lett.* 54: 2151
14. Fröhlich H. 1937. *Proc. R. Soc. London Ser. A* 160: 230
15. Shah J, Deveaud B, Damen TC, Tsang WT, Gossard AC, Lugli P. 1987. *Phys. Rev. Lett.* 59: 2222
16. Landsberg PT. 1991. *Recombination in Semiconductors*. Cambridge: Cambridge Univ. Press
17. Yoffa EJ. 1980. *Phys. Rev. B* 21: 2415
18. van Driel HM. 1987. *Phys. Rev. B* 35: 8166
19. Kalt H, Rinker M. 1992. *Phys. Rev. B* 45: 1139
20. Othonos A, van Driel HM, Young JF, Kelly PJ. 1991. *Phys. Rev. B* 43: 6682
21. Choo HR, Hu XF, Downer MC. 1993. *Appl. Phys. Lett.* 63: 1507
22. Wood RF, White CW, Young RT, eds. 1984. *Semiconductors and Semimetals*. Vol. 23. New York: Academic
23. Malvezzi AM, Kurz H, Bloembergen N. 1985. See Ref. 2, pp. 75–80
24. Malvezzi AM. 1987. In *Excited-State Spectroscopy in Solids*, ed. UM Grassano, N Terzi, pp. 335–54. Amsterdam: North-Holland Physics
25. Van Vechten JA, Tsu R, Saris FW. 1979. *Phys. Lett.* 74A: 422
26. Van Vechten JA. 1984. In *Semiconductors Probed by Ultrafast Laser Spectroscopy*, ed. RR Alfano, p. 95. San Diego: Academic
27. Li KD, Fauchet PM. 1983. *Appl. Phys. Lett.* 51: 21
28. Kurz H, Bloembergen N. 1985. See Ref. 2, pp. 3–13
29. Shank CV, Yen R, Hirlimann C. 1983. *Phys. Rev. Lett.* 51: 900
30. Reitze DH, Zhang TR, Wood WM, Downer MC. 1990. *J. Opt. Soc. Am. B* 7: 84
31. Shank CV, Yen R, Hirlimann C. 1983. *Phys. Rev. Lett.* 50: 454
32. Downer MC, Fork RL, Shank CV. 1985. *J. Opt. Soc. Am. B* 2: 595
33. Tom HWK, Aumiller GD, Brito-Cruz CH. 1988. *Phys. Rev. Lett.* 60: 1438
34. Schröder T, Rudolph W, Govorkov SV, Shumai IL. 1990. *Appl. Phys. A* 51: 1438
35. Govorkov SV, Shumay IL, Rudolph W, Schroeder T. 1991. *Opt. Lett.* 16: 1013
36. Sokolowski-Tinten K, Schulz H, Bialkowski J, von der Linde D. 1991. *Appl. Phys. A* 53: 227
37. Saeta PN, Wang J, Siegal Y, Bloembergen N, Mazur E. 1991. *Phys. Rev. Lett.* 67: 1023
38. Reitze DH, Ahn H, Downer MC. 1992. *Phys. Rev. B* 45: 2677
39. Siegal Y, Glezer EN, Mazur E. 1994. *Phys. Rev. B* 49: 16 403
40. Greenaway DL, Harbeke G. 1968. *Optical Properties and Band Structure of Semiconductors*. Oxford: Pergamon
41. Siegal Y, Glezer EN, Huang L, Mazur E. 1995. In *Ultrafast Phenomena in Semiconductors*, ed. DK Ferry, HM van Driel. Bellingham, WA.: SPIE. In press
42. Siegal Y, Glezer EN, Mazur E. 1995. In *Femtosecond Chemistry*, ed. J Manz, L Wöste. Berlin: Verlag Chemie. In press
43. Kim DH, Ehrenreich H, Runge E. 1994. *Solid State Commun.* 89: 119
44. Biswas R, Ambegoakar V. 1982. *Phys. Rev. B* 26: 1980
45. Stampfli P, Bennemann KH. 1990. *Phys. Rev. B* 42: 7163
46. Stampfli P, Bennemann KH. 1993. *J. Phys. Condens. Matter* 5: A173 (Suppl.)
47. Froyen S, Cohen ML. 1983. *Phys. Rev. B* 28: 3258
48. Shen YR. 1984. *The Principles of Nonlinear Optics*. New York: Wiley & Sons
49. Akhmanov SA, Koroteev NI, Paitan

GA, Shumay IL, Galyautdinov MV, et al. 1983. *Opt. Commun.* 47: 202
50. Akhmanov SA, Emel'yanov VI, Koroteev NI, Seminogov VN. 1985. *Sov. Phys. USP* 28: 1084
51. Liu JM, Malvezzi AM, Bloembergen N. 1985. See Ref. 2, pp. 137–42
52. Siegal Y. 1994. *Time-resolved studies of laser-induced phase transitions in GaAs.* PhD thesis. Harvard Univ., Cambridge. 149 pp.
53. Akhmanov SA, Galyautdinov MV, Koroteev NI, Paityan GA, Khaibullin IB, et al. 1985. *Bull. Acad. Sci. USSR Phys. Ser.* 49: 86
54. Glezer EN, Siegal Y, Huang L, Mazur E. 1995. *Phys. Rev. B.* In press
55. Saeta PN. 1991. *Optical studies of ultrafast carrier dynamics in semiconducting materials.* PhD thesis. Harvard Univ., Cambridge. 167 pp.